The Glycerol-Dependent Metabolic Persistence of *Pseudomonas putida* KT2440 Reflects the Regulatory Logic of the GlpR Repressor

Pablo I. Nikel,[a] Francisco J. Romero-Campero,[b] Joshua A. Zeidman,[c] Ángel Goñi-Moreno,[a] Víctor de Lorenzo[a]

Systems and Synthetic Biology Program, Centro Nacional de Biotecnología (CNB-CSIC), Madrid, Spain[a]; Department of Computer Science and Artificial Intelligence, Universidad de Sevilla, Seville, Spain[b]; Massachusetts Institute of Technology, Cambridge, Massachusetts, USA[c]

ABSTRACT The growth of the soil bacterium *Pseudomonas putida* KT2440 on glycerol as the sole carbon source is characterized by a prolonged lag phase, not observed with other carbon substrates. We examined the bacterial growth in glycerol cultures while monitoring the metabolic activity of individual cells. Fluorescence microscopy and flow cytometry, as well as the analysis of the temporal start of growth in single-cell cultures, revealed that adoption of a glycerol-metabolizing regime was not the result of a gradual change in the whole population but rather reflected a time-dependent bimodal switch between metabolically inactive (i.e., nongrowing) and fully active (i.e., growing) bacteria. A transcriptional Φ(*glpD-gfp*) fusion (a proxy of the glycerol-3-phosphate [G3P] dehydrogenase activity) linked the macroscopic phenotype to the expression of the *glp* genes. Either deleting *glpR* (encoding the G3P-responsive transcriptional repressor that controls the expression of the *glpFKRD* gene cluster) or altering G3P formation (by overexpressing *glpK*, encoding glycerol kinase) abolished the bimodal *glpD* expression. These manipulations eliminated the stochastic growth start by shortening the otherwise long lag phase. Provision of *glpR* in *trans* restored the phenotypes lost in the Δ*glpR* mutant. The prolonged nongrowth regime of *P. putida* on glycerol could thus be traced to the regulatory device controlling the transcription of the *glp* genes. Since the physiological agonist of GlpR is G3P, the arrangement of metabolic and regulatory components at this checkpoint merges a positive feedback loop with a nonlinear transcriptional response, a layout fostering the observed time-dependent shift between two alternative physiological states.

IMPORTANCE Phenotypic variation is a widespread attribute of prokaryotes that leads, *inter alia*, to the emergence of persistent bacteria, i.e., live but nongrowing members within a genetically clonal population. Persistence allows a fraction of cells to avoid the killing caused by conditions or agents that destroy most growing bacteria (e.g., some antibiotics). Known molecular mechanisms underlying the phenomenon include genetic changes, epigenetic variations, and feedback-based multistability. We show that a prolonged nongrowing state of the bacterial population can be brought about by a distinct regulatory architecture of metabolic genes when cells face specific nutrients (e.g., glycerol). *Pseudomonas putida* may have adopted the resulting carbon source-dependent metabolic bet hedging as an advantageous trait for exploring new chemical and nutritional landscapes. Defeating such naturally occurring adaptive features of environmental bacteria is instrumental in improving the performance of these microorganisms as whole-cell catalysts in a bioreactor setup.

The customary view of prokaryotic metabolism as a homogeneous and cooccurring process in space and time has been increasingly challenged in recent years (1, 2), particularly since the onset of single-cell technologies (3–6). These methodologies revealed a complete repertoire of responses to specific environmental conditions in individual microorganisms (7–12). Diversification of the metabolic regimes in single cells within otherwise clonal populations can be seen as a particular case of phenotypic variation (13, 14), in which different regulatory or epigenetic traits lead to the stochastic manifestation of alternative features in isogenic individuals (15–19). The phenomenon known as persistence, i.e., the occurrence of a live but nongrowing fraction of cells in a bacterial pool (20), is one of the most intriguing cases of

phenotypic variation. While the lack of growth may appear negative at a glance, persistence ensures the survival of cells exposed to agents that act on developing bacteria, e.g., some antibiotics (21–23). Once the selective pressure ceases, persistent bacteria can resume growth and fully reconstruct the original population. Regardless of the mechanisms behind this behavior, the standing question is whether persistence is an adaptive trait or just a casual occurrence that happens to be beneficial for antibiotic-sensitive bacteria in the modern era of antimicrobial agents. What we qualify as persistence may just be a particular case of a more common situation in which a starting population stochastically splits between growing and nongrowing cell types when facing a new environmental or physicochemical condition. While persistence re-

flects the end of one such scenario (most bacteria grow but a few fail to grow), the opposite extreme (most cells remain static but a few grow) could also occur.

During the course of our studies on the metabolism of the soil bacterium *Pseudomonas putida* KT2440, we noticed that cells cultured on glycerol as the sole carbon source displayed an anomalously long lag period (≥10 h) before initiating any detectable growth. This situation was not observed when the cells were cultured on glucose or succinate under the same conditions. Much of the currently available information on glycerol metabolism in pseudomonads comes from studies of the human pathogen *Pseudomonas aeruginosa* (24, 25), and only recently have the transcriptional and metabolic changes associated with the growth of *P. putida* KT2440 on glycerol been assessed (26). Cells grown on the polyol undergo a complex transcriptional response that includes not only genes involved in central metabolic pathways but also additional ones encoding components of the respiratory chain and others related to stress resistance (27). Yet, the body of data currently available does not provide any clue on the distinct long-lag-phase phenomenon in glycerol. Since this behavior is recurrent upon reinoculation of the cells in fresh medium, we wondered whether the prolonged nongrowing regime of *P. putida* on glycerol was the result of (i) a lengthy, graded, and simultaneous adaptation to the new substrate or (ii) a runaway counterpart of persistence, i.e., the stochastic rise and eventual population takeover of individual substrate-metabolizing cells amid a majority of glycerol-unresponsive bacteria.

In this work, we present a systematic study of the growth and physiology of individual *P. putida* KT2440 cells in cultures with the polyol as the sole carbon source. In particular, we show that exposure to glycerol led to the appearance of two clearly separate subpopulations that differed in their metabolic activity toward the substrate, where the relative proportion of these subpopulations changed with time. Furthermore, such a phenotypic diversification was wired to the dual logic of the GlpR regulator, which represses transcription of the cognate *glp* genes encoding the enzymes needed for glycerol catabolism. Our results suggest that the metabolic heterogeneity observed in glycerol cultures could be an evolutionary trait of *P. putida*, endowing the bacterium with bethedging strategies for scouting new substrates-to-be in natural ecological niches.

RESULTS AND DISCUSSION

Glycerol consumption pathways in *P. putida* KT2440 exposed by the genomic organization of the *glp* locus. Two glycerol dissimilation pathways have been described in bacteria: one begins with a dehydrogenation step, followed by phosphorylation, and the other begins with a phosphorylation reaction, followed by dehydrogenation (28, 29). In either case, the terminal metabolic currency is dihydroxyacetone-P. In the soil bacterium *P. putida* KT2440, the second pathway is the prevalent (and likely the only) glycerol dissimilatory process (Fig. 1). Uptake of the compound is mediated by the GlpF facilitator, which fosters a diffusion reaction (30). Once inside the cell, glycerol is phosphorylated by an ATP-dependent glycerol kinase (GlpK) to *sn*-glycerol-3-P (G3P), which cannot diffuse out of the cell. G3P is the substrate for GlpD, a membrane-bound G3P dehydrogenase that yields dihydroxyacetone-P (Fig. 1A). Some microorganisms, such as *Escherichia coli* and *P. aeruginosa*, are able to internalize and utilize G3P or dihydroxyacetone (28), intermediates of the biochemical polyol
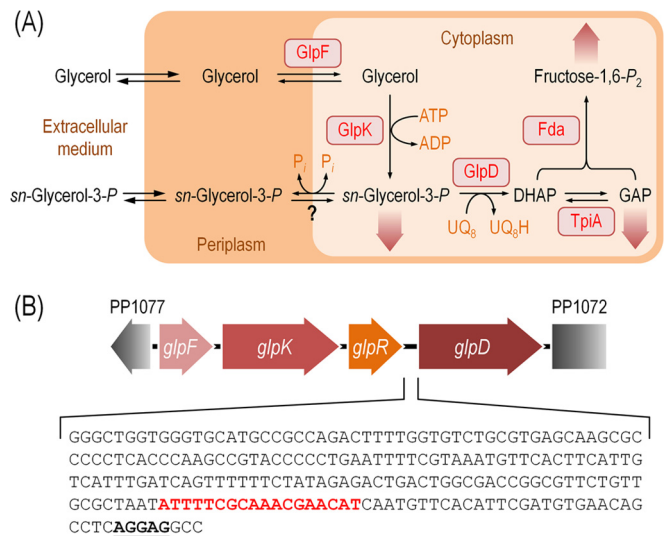

FIG 1 (A) Glycerol metabolism in *Pseudomonas putida* KT2440. The initial steps in the conversion of the polyol into intermediates of the central metabolism are shown along with the enzymes that catalyze these steps. Upon entrance of glycerol into the cytoplasm (mediated by GlpF, the glycerol facilitator), it is used as the substrate of GlpK (glycerol kinase). Glycerol-3-P is then oxidized in an ubiquinone-dependent reaction catalyzed by the membrane-bound GlpD (*sn*-glycerol-3-P dehydrogenase). Dihydroxyacetone-P (DHAP) formed therein enters into the central metabolic pathways through the activity of TpiA (triosephosphate isomerase, which establishes an equilibrium between DHAP and glyceraldehyde-3-P [GAP]) and Fda (fructose-1,6-P_2 aldolase). Further metabolic steps are indicated in this outline with wide shaded arrows. The question mark below the arrows corresponding to *sn*-glycerol-3-P transport indicates that no such transporter has been identified in strain KT2440. (B) Genetic organization of the *glp* locus. The genomic region encompasses *glpF* (PP1076, a major intrinsic protein [MIP] family channel protein), *glpK* (PP1075, glycerol kinase), *glpR* (PP1074, a DeoR family transcriptional regulator), and *glpD* (PP1073, glycerol-3-P dehydrogenase). The entire cluster is flanked upstream by PP1072, encoding an uncharacterized hypothetical protein, and downstream by PP1077, encoding a YbaK/EbsC-type protein (prolyl-tRNA editing protein). Note that the elements in this outline are not drawn to scale. The 5′ untranslated region preceding the *glpD* gene is shown along with the predicted *glpD* promoter (red) and a putative Shine-Dalgarno signal (boldface, underlined).

processing (Fig. 1A). The activities are encoded in *P. putida* by the *glp* gene cluster (26, 31), which includes *glpF*, *glpK*, *glpR*, and *glpD* (Fig. 1B). Deep RNA sequencing indicated that *glpR* is constitutively transcribed at a low level in the whole bacterial population irrespective of the carbon source, while the rest of the *glp* genes have a significant expression level only in glycerol cultures (27). Coverage plots demonstrated that there are two transcriptional units within the *glp* gene cluster: one transcriptional unit encompasses *glpF* and *glpK*, and *glpD* is independently transcribed (27). All of these genes are under the transcriptional control of the negative regulator GlpR, a regulatory arrangement previously described in other bacteria (32–34). *In silico* predictions have suggested that the promoters of the *glp* regulon share a regulatory motif in Gram-negative bacteria (35), and on the basis of this feature, we were able to recognize a well-defined GlpR-binding sequence upstream of *glpD* (Fig. 1B). Danilova et al. (35) also hinted at the existence of more GlpR-binding motifs upstream of genes relevant for glycerol uptake and utilization but not upstream of *glpR*. Against this background, we examined how all

these biochemical and genetic features of *P. putida* KT2440 bring forth a distinctive growth phenotype on glycerol.

Behavior of single *P. putida* KT2440 cells growing on glycerol. When *P. putida* is grown on glycerol as the sole carbon source, the cultures show an unexplainably prolonged lag phase that typically lasts ≥10 h (26, 31). The conspicuously long time needed to start growth is independent of the carbon source used to grow the inocula and almost disappears (1.5 ± 0.9 h) only when cells are pregrown on the polyol. The lag phase lasted for 17.4 ± 3.9 h and 19.8 ± 2.4 h when cells were transferred from either succinate or glucose cultures into a glycerol-containing medium, respectively. Interestingly, the addition of substrate mixtures (e.g., glucose and glycerol) to the cultures helps reduce the extension of the lag phase. This situation indicates that a metabolic regulatory phenomenon (e.g., the accumulation of a critical metabolic intermediate) could be involved in the delayed growth on glycerol. Since the growth retardation was even more noticeable when *P. putida* was pregrown in rich LB medium and then passed into M9 minimal medium containing glycerol (the lag phase lasted >20 h), we adopted this culture approach in all the experiments described in this study. A considerable reorganization of metabolic pathways is expected to occur when cells are shifted from rich to minimal growth conditions (36), including changes in gene expression during the lag phase (37). However, the unexpectedly long lag phase of strain KT2440 on glycerol cannot be easily explained. What are the metabolic and regulatory causes behind such delayed growth of *P. putida* on the polyol?

The first aspect to be addressed was whether (i) the growth retardation applied to all cells of the culture in a more or less synchronous fashion or (ii) what we observed at the population level in reality reflected a stochastic start of growth of individual cells. We monitored the evolution of separate cultures of *P. putida* in microtiter plates inoculated with a dilution of a bacterial suspension that corresponded to an average of 1 cell per well (Fig. 2). Cells previously cultured in LB medium were used as the inoculum, and after washing them with M9 minimal medium without any carbon source (to remove any traces of the complex medium), we transferred the bacteria into M9 minimal medium supplemented with either glucose (i.e., glycolytic substrate), succinate (i.e., gluconeogenic substrate), or glycerol (in which cells adopt a mixed metabolic regime recruiting both gluconeogenic and glycolytic metabolic activities [26]). Inocula were diluted in such a way that each culture (in 96-well microtiter plates) was calculated to receive 1 cell (see Materials and Methods for details on numerical considerations). Growth in each well was periodically monitored as the change in optical density measured at 600 nm (OD_{600}), and results from 1,000 wells were analyzed to ensure a data set large enough to have statistical significance. Figure 2A reveals various informative features. First, the lag phase differed significantly between cultures using different carbon sources (26). Cells started to grow on glucose or succinate in an almost synchronous fashion (data not shown). In contrast, glycerol cultures starting from single cells per well showed a remarkable variation in the extension of the lag phase. Second, once bacterial growth started, the specific growth rate (μ_{max}) for a given carbon source was virtually identical among all individual wells. Succinate promoted the fastest growth ($\mu_{max} = 0.43 \pm 0.07$ h^{-1}), closely followed by glucose ($\mu_{max} = 0.39 \pm 0.06$ h^{-1}) and then by glycerol ($\mu_{max} = 0.24 \pm 0.05$ h^{-1}). These results qualitatively mirror the behavior of *P. putida* growing in these carbon sources in shaken-flask cul-
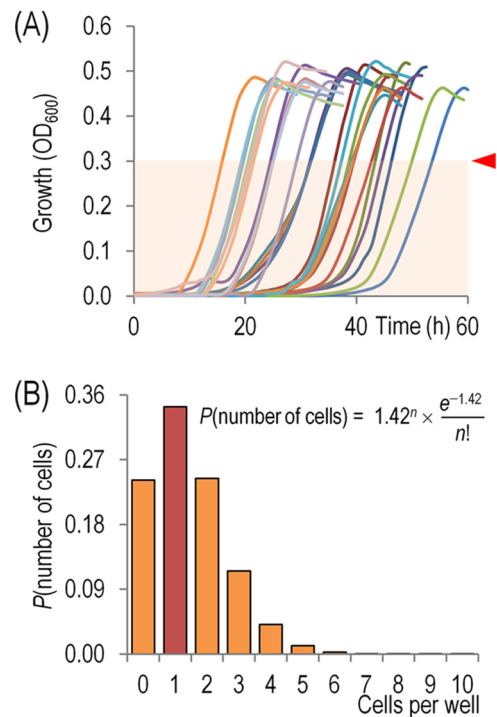

FIG 2 (A) Growth of *P. putida* KT2440 in single-cell batch cultures. Multiwell microtiter plates were inoculated with a highly diluted preculture previously developed in LB medium in order to start each culture from 1 cell per well. Cells were grown at 30°C in 200 μl of M9 minimal medium containing 40 mM glycerol with rotary agitation. The time needed to reach an optical density measured at 600 nm (OD_{600}) of 0.3 (mid-exponential phase of growth) is indicated by a red arrowhead for 50 independent cultures to illustrate the delay in growth initiation among individual wells. This parameter, termed time of metabolic response (t_{MR}), was further used to quantify the response of single-cell cultures. (B) Probability of inoculating a given number of cells in a particular well, as estimated by the Poisson probability distribution. After dilution and inoculation, and due to stochastic variations (e.g., small differences in the volume of the bacterial suspension transferred into each well), the number of cells per well (n) is not exactly known and may vary from well to well. The probability P of inoculating zero, one, two, or three cells per well is shown, indicating that the probability of inoculating a single cell is the most likely outcome.

In figure B: $$P(\text{number of cells}) = 1.42^n \times \frac{e^{-1.42}}{n!}$$

tures and using a larger inoculum (26). Regardless of the extension of the lag phase and the individual μ_{max} values, all individual samples reached more or less the same maximal OD_{600} values (in the case of glycerol cultures, ca. 0.5 to 0.6 units).

These results made us wonder whether the asynchronous distribution of growth curves on glycerol (Fig. 2A) could be just the spurious consequence of differences in the initial number of cells per well. In other words, we questioned whether the observed phenomenon might be related to the manipulation of the cells rather than arising from physiological or genetic traits. Due to stochastic variations in the experimental procedure (e.g., differences in the inoculum volume transferred into the wells), the number of cells per well is not exactly known and may vary from well to well. Assuming that (i) the number of cells per well is proportional to its volume, (ii) the probability of having two cells in an infinitesimal volume is negligible, and (iii) inoculating a given number of cells is independent from the particular well considered, the Poisson probability distribution (38) can be used to

theoretically assess the number of cells which can be expected per well (see Materials and Methods). Figure 2B shows that the probability of inoculating zero, one, two, or three cells per well is appreciable, whereas the probability of inoculating more than four cells is negligible. Inoculating a single cell per well is the most likely outcome ($P = 0.343$), and consequently, the growth pattern observed in each well can be associated with a sole *P. putida* cell. The possibility of inoculating more than 1 cell is not to be neglected, but we show that our observations are not produced by the initial variability in the number of cells per well (see below).

Single *P. putida* KT2440 cells grown on glycerol undergo different metabolic regimes. The results described above raised the question of how individual cells within a *P. putida* KT2440 population react metabolically to exposure to different carbon sources. The gross physiological state of single cells in shaken-flask cultures was examined to study this issue. Since a large number of bacterial oxidases and reductases are involved in central enzymatic functions, the merged redox activity of a cell can be considered a proxy of its overall physiological vitality. On this background, the *Bac*Light RedoxSensor Green vitality stain, 3,8-diamino-5-[3-(diethylmethylammonio)propyl]-6-phenyl di-iodide (RSG reagent), was used to diagnose the metabolic state of individual cells. This reagent can be transformed by cell reductases into a highly fluorescent compound, a reliable descriptor of changes in the electron transport chain activity and other vital cellular processes (39, 40). As such, the metabolic heftiness of individual cells could be directly related to the intensity of the RSG signal (17). We stained *P. putida* cells harvested during mid-exponential growth from shaken-flask cultures with the same carbon sources described above. Bacteria were precultured in LB medium, washed with M9 minimal medium without any carbon source, and then passed into fresh M9 minimal medium supplemented with either succinate, glucose, or glycerol. Mid-exponential cultures were harvested at an OD_{600} of 0.5 (note that the duration of the lag phase was different for each carbon source [26]), and cells were stained with the RSG reagent and inspected under the fluorescence microscope. The distribution of RSG-stained cells revealed different patterns depending on the substrate used (Fig. 3). On one hand, the relative intensity of RSG staining increased in the order glycerol < glucose << succinate. On the other hand, the same cell-bound signals appeared to be homogeneously distributed in the population of bacteria grown on glucose and succinate but not so in the glycerol-grown counterpart. No significant signal was observed in cells not treated with the RSG reagent, ensuring that the observed fluorescence stems from redox activity and not from autofluorescence or siderophore production (41). While small cell-to-cell differences in the RSG output of the glucose- and succinate-grown cultures can be considered normal, the clear divide between different metabolic states exposed by the data in Fig. 3 (bottom panel) prompted us to reexamine the case in more detail by means of flow cytometry. This method not only allows for the quantitation of the fluorescent signal in single cells but also enables the recognition of distinct subpopulations (42). Quantitative image analysis of the fluorescence microscopy pictures of Fig. 3 further exposes the cell-to-cell variability observed in terms of RSG staining in glycerol cultures but not in glucose or succinate cultures (see also Fig. S1 in the supplemental material).

Figure 4 shows the results obtained by flow cytometry of cells from the same shaken-flask cultures described above. In order to validate the positive correlation between RSG staining and metabolic activity of individual cells, samples from each culture condition were either treated with NaN_3 or heated at 85°C for 25 min to
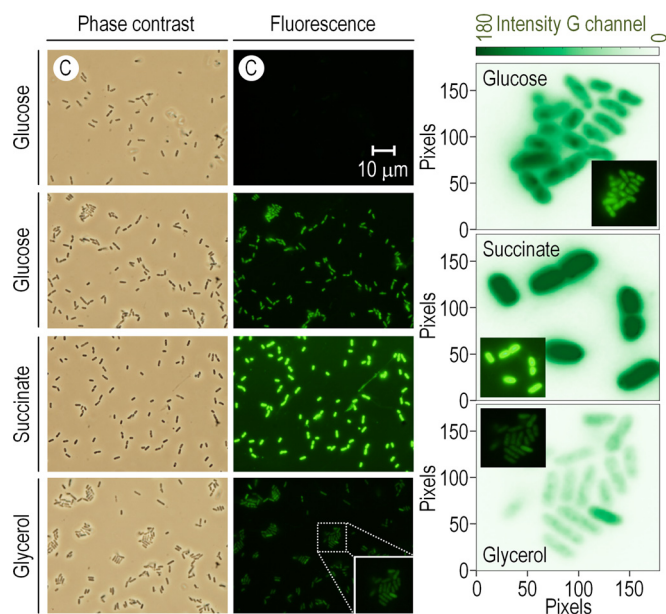

FIG 3 Fluorescence microscopy exploration and image analysis of the *Bac*Light RedoxSensor Green (RSG) signal in *P. putida* KT2440 grown on different carbon sources. Bacteria were grown in shaken-flask cultures using M9 minimal medium supplemented with the indicated carbon sources, and cells were harvested during mid-exponential growth (corresponding to an optical density measured at 600 nm of 0.5). Bacteria were stained with the RSG reagent as recommended by the manufacturer and observed under the microscope as detailed in Materials and Methods. The first two columns at the left of the figure show the microscopy pictures. The top panels indicate a control experiment (C), in which cells were not stained (note that only glucose-grown cells are shown in these panels; the same control experiment performed with cells grown on succinate or glycerol gave similar results in terms of background fluorescence). A closeup of a group of glycerol-grown *P. putida* cells is shown in the bottom panel to illustrate the differences in the level of fluorescence among individual bacteria. The accompanying image analysis shows two-dimensional plots of the RSG staining intensity as quantified in the output of the green (G) channel. Groups of cells were randomly selected from the fluorescence microscopy pictures for each carbon source (as indicated in the insets). In the case of cells from glycerol cultures, the cluster shown in the closeup inset of the fluorescence microscopy picture was subjected to quantitative image analysis. The background green fluorescence was subtracted from each two-dimensional plot.

inactivate the cells. In either case, *P. putida* KT2440 showed no RSG signal in flow cytometry and cells were indistinguishable from the unstained control irrespective of the carbon source (data not shown). Various types of RSG-staining patterns quickly developed in live cells. First, as observed under the fluorescence microscope (Fig. 3), no significant differences were noticed in either the apparent size or the complexity of individual cells irrespective of the carbon source (i.e., forward scatter versus side scatter plots; Fig. 4, left panels). Second, bacteria grown on glucose or succinate were all positive for RSG staining and thus originated a single peak of fluorescence that was clearly displaced from the negative (unstained) control. This situation indicates that all cells were actively metabolizing the substrates on which they were growing. The unimodal distribution of RSG^+ signals and their intensity matched the fluorescence microscopy data of Fig. 3, with *P. putida* cells from succinate cultures giving the highest output. In contrast to cultures developed under entirely glycolytic or gluconeogenic regimes, when cells grew on glycerol a sharp divide of the bacterial
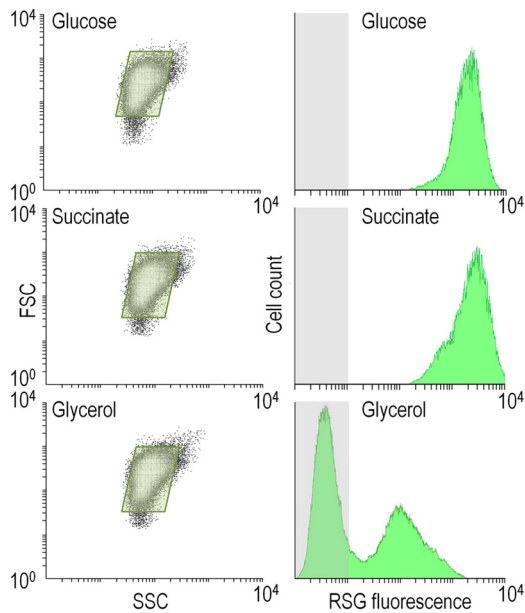
FIG 4 Flow cytometry analysis of the *Bac*Light RedoxSensor Green (RSG) signal in *P. putida* KT2440 growing on different carbon sources. Cells were grown in shaken flasks until they reached the mid-exponential phase of growth and were treated with RSG as indicated in the legend to Fig. 3, and the fluorescence intensity was quantified by flow cytometry. The gated population, in which the RSG signal was investigated, is indicated in the forward scatter (FSC) versus side scatter (SSC) plots (left column). The histograms in the right column show the distribution of RSG fluorescence in cells harvested from glucose, succinate, and glycerol cultures. The gray rectangle in each histogram plot identifies the region considered negative for the fluorescence signal (as assessed with unstained cells).
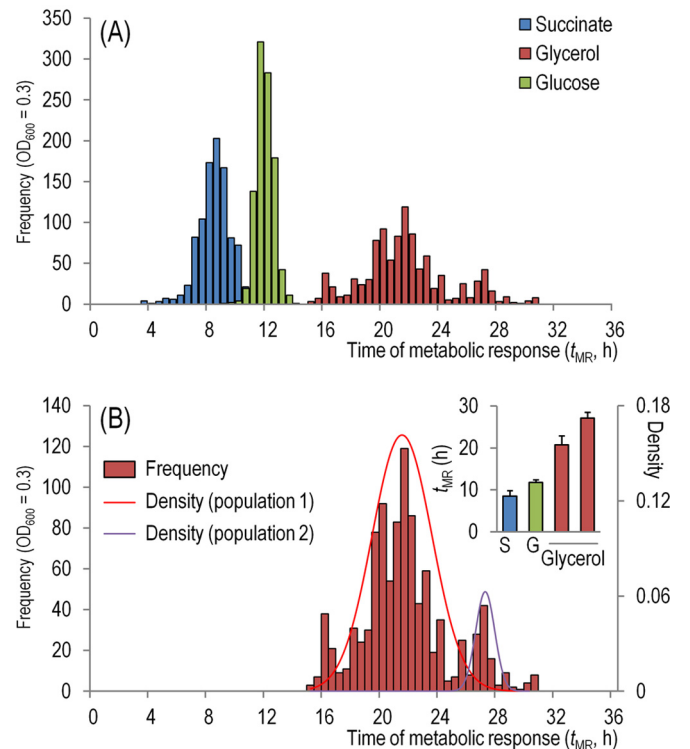

FIG 5 (A) Frequency distribution of the time of metabolic response (t_{MR}, defined as the time needed for a given culture to attain an optical density measured at 600 nm [OD_{600}] of 0.3) in 1,000 single-cell *P. putida* KT2440 cultures carried out in microtiter plates with different carbon sources as described in the legend to Fig. 2. The bars indicate the number of independent wells in which the cultures attained an OD_{600} of 0.3 at a given t_{MR}. (B) Closeup of the frequency of t_{MR} values observed in glycerol cultures. The calculated Gaussian distributions are superimposed on the bar graph to identify the possible subpopulations under these conditions (see also Table S2 in the supplemental material). The inset indicates the absolute values of the t_{MR} derived from the distribution shown in panel A for succinate (S), glucose (G), and glycerol cultures. Note that in the case of glycerol cultures, there are two values corresponding to the subpopulations observed under these conditions. In the inset, each bar represents the mean value of the t_{MR} parameter ± SD.

population into two groups became apparent. The two subpopulations differed in their degree of staining: 62% of the cells were RSG$^+$, while the remaining 38% exhibited almost no fluorescence (Fig. 4, bottom panel). One of the subpopulations virtually overlapped with the negative (i.e., unstained) control experiment, meaning that these cells lacked any significant metabolic activity and can be considered metabolically dormant. The divide was consistently observed throughout the mid-exponential phase of growth but tended to gradually merge as a single bacterial pool of metabolically active cells (i.e., most of the cells became RSG$^+$) as the growth progressed and the cultures moved into the late exponential phase (see Fig. S2 in the supplemental material).

These results provide a direct link between the time-dependent metabolic bimodality of single cells grown in glycerol and the macroscopically observed lag phase of the corresponding batch cultures. Since the bimodal behavior of RSG$^+$ *P. putida* cells was observed only in glycerol cultures and not in the presence of glucose or succinate, we hypothesized that the bifurcation was connected to the metabolism of the polyol itself. However, such plausible connection was by no means evident in the physiological experiments conducted so far, and we therefore set out to explore it with a suite of genetic and biochemical approaches.

Quantitative analysis of growth patterns. To analytically study the growth pattern under different culture conditions, we defined a kinetic parameter, termed time of metabolic response (t_{MR}). This parameter is the time needed by a given single-cell culture to attain an OD_{600} of 0.3, which is roughly half the maxi-

mal cell density observed in glycerol cultures in microtiter plates (Fig. 2A). Note that the very definition of t_{MR} merges both the kinetics of cell growth and the extent of the lag phase. This concept is reminiscent of the parameters used for describing the dynamic behavior of regulatory transcriptional networks (43, 44). The characteristic t_{MR} values were recorded for each well in 1,000 independent cultures, and their absolute frequency was plotted against time, resulting in Gaussian-like distributions that were clearly unimodal for cells growing on either succinate or glucose as the carbon source (Fig. 5A). In sharp contrast, glycerol cultures had a multimodal distribution of t_{MR} values, hinted at by a scattered distribution of frequencies. Yet, is this distribution composed by more than one subpopulation, as intimated by visual inspection of Fig. 5A? To answer this question, we resorted to model-based unsupervised clustering to identify possible subpopulations. According to Table S2 in the supplemental material, two different subpopulations can be discerned according to their characteristic t_{MR} values. A first subpopulation comprised 89% of the entire population and exhibited an average t_{MR} of 23.7 ± 2.2 h,

whereas a second subpopulation comprised 11% of the entire population and had a t_{MR} of 29.8 ± 0.7 h (Fig. 5B). Furthermore, the application of these statistical methodologies to data from succinate and glucose cultures revealed a single population for each condition, as expected from the results in Fig. 5A. In other words, our statistical analysis identified two subpopulations in glycerol cultures, clearly distinguishable by their characteristic t_{MR} values (Fig. 5B, inset). These results, in turn, correlate well with the bimodal distribution of cells differing in their metabolic activity (Fig. 4). We simulated a scenario where the only source of stochasticity was the initial number of cells and obtained a unimodal distribution of t_{MR} values (see Fig. S3 in the supplemental material). Once the phenomenon of metabolic bimodality on glycerol (which results in a stochastic distribution of growth initiation of single cells and a population-level prolonged lag phase) was well documented, the next question related to the underlying molecular mechanism.

The GlpR repressor imposes a bistable growth pattern of cells grown on glycerol. Inspection of the biochemical and regulatory components underlying glycerol utilization in *P. putida* (Fig. 1A and B) and comparison of the same elements in other bacteria reveal important information about the use of this polyol by Gram-negative bacteria (45). It can be seen that (i) the *glp* structural genes are under the transcriptional control of a single regulatory protein (i.e., GlpR), known to act as a transcriptional repressor (34, 35); (ii) G3P seems to be the key metabolite that relieves the GlpR-dependent repression of the *glp* gene cluster (28); (iii) since G3P is not a substrate of the GlpF facilitator (30, 46), it can neither be taken up by *P. putida* cells nor leaked to the surrounding medium; and (iv) the very driving force for glycerol uptake thus arises from substrate phosphorylation by GlpK. Not surprisingly, this particular arrangement of regulatory elements is reminiscent of other genetic systems known to be submitted to stochastic fluctuations, such as the *lac* operon in *E. coli* (see below).

A typical bistable behavior at the transcriptional level is imposed by a repressor protein on the transcription of regulated genes (16, 18). The underlying mechanism proposed to explain bistability assumes a specific feedback that acts in combination with a nonlinear response within a transcriptional network (14). The archetypal example in this sense is the *lac* operon of *E. coli*, in which the LacI repressor sets a bimodal expression pattern on the cognate genes (47); the same goes for the structure of the *glp* genes in *P. putida*. Within this framework, it seems likely that the GlpR regulator and the *glp* genes comprise a genetic system prone to exhibiting a bistable regime. To explore this possibility, we eliminated the *glpR* gene in *P. putida* KT2440 (which would determine the constitutive expression of the *glp* genes) and we studied the phenotypic traits discussed in the sections above in the mutant strain.

The first indication of the involvement of GlpR in the bistable growth phenotype of *P. putida* came from shaken-flask culture experiments with the Δ*glpR* mutant using glycerol as the carbon source. Cells used as the inoculum were grown in LB medium. The duration of the lag phase was reduced to 6.5 ± 1.7 h (i.e., approximately 16 h shorter than the lag phase observed for the wild-type strain under the same culture conditions). We then focused on the catabolic enzymes involved in glycerol utilization (Fig. 6A), and we measured the GlpK activity *in vitro* to study the effect of eliminating GlpR in strain KT2440. Figure 6B shows that the GlpK

activity is highly responsive to the carbon source. Wild-type cells growing under a glycolytic metabolic regime had the lowest GlpK activity, although the level of enzymatic activity was distinguishable from the background (attaining 7.5 ± 2.5 nmol · min^{-1} · mg protein^{-1}). The *in vitro* GlpK activity increased ca. 5-fold when *P. putida* cells were cultured on glycerol, as reported previously (26). However, the specific GlpK activity in the Δ*glpR* strain did not react to the carbon source used to grow the cells. The GlpK activity was detectable even in mutant cells grown in LB medium (data not shown), a culture condition under which the same enzymatic activity was almost completely repressed in the wild-type strain. These results indicate that the elimination of the GlpR repressor protein renders the expression of *glpK* (and therefore the cognate enzymatic activity) constitutive. Moreover, elimination of GlpR completely abolished the bistable growth phenotype, and the entire subpopulation now showed a unimodal behavior (Fig. 6C). This evidence would in principle suffice to explain the observed phenotype of *P. putida* KT2440 on glycerol, and it also provides a biochemical clue to its origin. As an additional control experiment designed to ascribe the bistable growth behavior to the GlpR repressor, we cloned the cognate gene in the low-copy-number pSEVA224 expression vector (giving rise to plasmid pE-*glpR* [Table 1]), and the Δ*glpR* strain was complemented back. The expression of *glpR* in *trans* restored the stochastic profile of growth (Fig. 6C and D), causing a significant decrease in the *in vitro* GlpK activity (8.7 ± 1.9 nmol · min^{-1} · mg protein^{-1}, comparable to the activity observed in the wild-type strain under similar growth conditions). The results accredit the role of GlpR as a transcriptional repressor of the cognate *glp* genes and suggest that the delayed growth of part of the bacterial cells is related to a limited activity of the catabolic enzymes encoded therein.

Time-dependent transcription of the *glp* genes as a descriptor of the macroscopic phenotype on glycerol. In an attempt to correlate the regulation of the *glp* genes and the phenotype observed in glycerol cultures, we constructed a transcriptional Φ(*glpD-gfp*) fusion based on the green fluorescent protein (GFP) to assess the *glpD* expression level (Fig. 7A). In this construct, the native promoter and the Shine-Dalgarno sequence of *glpD* were placed before *gfp* (in the pSEVA637 vector) to drive its expression. In these experiments, *P. putida* KT2440 cells carrying the Φ(*glpD-gfp*) reporter (plasmid pTF-*glpD* [Table 1]) were grown on glycerol in shaken-flask cultures, and broth samples were taken at selected time points to study gene expression by flow cytometry. Note that, besides a negative control (Fig. 7B), the data points at which cells were collected correspond to the lag phase (8 h, Fig. 7C), mid-exponential phase (18 h, Fig. 7D), and stationary phase (36 h, Fig. 7E), reflecting different physiological situations as the bacteria proceed through the growth curve. Figure 7C to E summarizes the evolution of the *glpD* transcriptional activity in strain KT2440 carrying pTF-*glpD* over time. At 8 h, before cells had started noticeable growth, most of the bacteria were negative for Φ(*glpD-gfp*) transcription, although a small subpopulation of GFP$^+$ cells was consistently detected (accounting for <20% of the total population; Fig. 7C). After 18 h of glycerol-dependent growth, when cells were actively growing, the separation of two subpopulations in terms of GFP content was still evident (Fig. 7D), although the percentage of GFP$^+$ cells under these circumstances increased to 57%. Moreover, the analytical deconvolution of the flow cytometry histogram indicated that the whole signal was the result of two overlapped Gaussian distributions
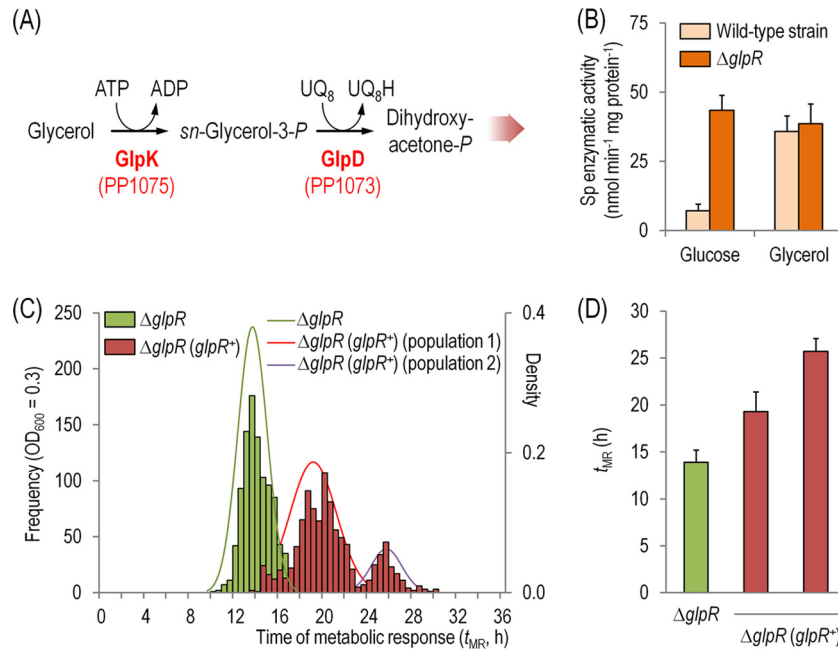
FIG 6 (A) Glycerol catabolic pathway in *P. putida* KT2440. Upon uptake of the substrate by the GlpF facilitator, it is phosphorylated by GlpK (glycerol kinase) and the resulting intermediate is further oxidized by GlpD (*sn*-glycerol-3-P dehydrogenase), which uses ubiquinone (UQ_8) as the cofactor (26) to yield dihydroxyacetone-P. This metabolite finally enters into the central catabolism, as indicated by a shaded arrow. (B) *In vitro* quantitation of the specific (Sp) GlpK enzymatic activity of cells grown in shaken-flask cultures on M9 minimal medium supplemented with either glucose or glycerol. Cells were harvested in the mid-exponential phase of growth (OD_{600} of 0.5), and the activity of GlpK was determined in the cell extract as detailed in Materials and Methods. Each bar represents the mean value of the corresponding enzymatic activity ± standard deviation of duplicate measurements from at least three independent experiments. (C) Distribution of the time of metabolic response (t_{MR}) in 1,000 single-cell cultures (carried out as described in the legend to Fig. 2 and using glycerol as the sole carbon source) for *P. putida* KT2440 Δ*glpR* and its complemented derivative (termed the Δ*glpR glpR*+ strain, which carries plasmid pE-*glpR*). The calculated Gaussian distributions are superimposed on the bar graph to identify possible subpopulations under these culture conditions. (D) Absolute values of the t_{MR} parameter in glycerol cultures, as derived from the distribution shown in panel C. Note that in the case of the cultures of the complemented strain, there are two values corresponding to the subpopulations observed under these culture conditions. Each bar represents the mean value of the t_{MR} value ± standard deviation.

(Fig. 7D, inset). This analysis indicates that the GFP− and GFP+ populations represent 35% and 65% of the total fluorescence signal in the histogram, respectively. When cells attained the early stationary phase (Fig. 7E), all of them were GFP+ in a unimodal distribution. Interestingly, the *glpD* expression pattern qualitatively mirrored the distribution of metabolically active and inactive cells (Fig. 4; see also Fig. S2 in the supplemental material).

The experimental evidence so far indicated that GlpR is ulti-

TABLE 1 Bacterial strains and plasmids used in this work

Bacterial strain or plasmid	Relevant characteristics[a]	Reference or source
Strains		
Escherichia coli		
CC118 λ*pir*	Cloning host; Δ(*ara-leu*) *araD* Δ*lacX174 galE galK phoA thiE1 rpsE rpoB* (Rif^r) *argE*(Am) *recA1* λ*pir* lysogen	80
HB101	Helper strain; F− λ− *hsdS20*(r_B− m_B−) *recA13 leuB6*(Am) *araC14* Δ(*gpt-proA*)62 *lacY1 galK2*(Oc) *xyl-5 mtl-1 thiE1 rpsL20*(Sm^r) *glnX44*(AS)	81
Pseudomonas putida		
KT2440	Wild-type strain; mt-2 derivative cured of the TOL plasmid pWW0	48, 82
KT2440 Δ*glpR*	KT2440 derivative; in-frame deletion of the *glpR* gene	This work
Plasmids		
pRK600	Helper plasmid used for conjugation; *ori*(ColE1), RK2(*mob*+ *tra*+); Cm^r	83
pSEVA637	Cloning vector; *ori*(pBBR1), promoter-less *gfp*; Gm^r	84, 85
pTF-*glpD*	pSEVA637 derivative with a DNA fragment corresponding to the 5′ UTR of *glpD*, including the *glpD* promoter and Shine-Dalgarno sequence, cloned before the *gfp* gene [Φ(*glpD-gfp*)]; Gm^r	This work
pSEVA224	Expression vector; *ori*(R2K); Km^r	84, 85
pE-*glpR*	pSEVA224 derivative carrying *glpR*; Km^r	This work
pE-*glpFK*	pSEVA224 derivative carrying *glpF* and *glpK*; Km^r	This work

[a] Antibiotic markers: Cm, chloramphenicol; Gm, gentamicin; Km, kanamycin; Rif, rifampin; Sm, streptomycin; 5′ UTR, 5′ untranslated region.
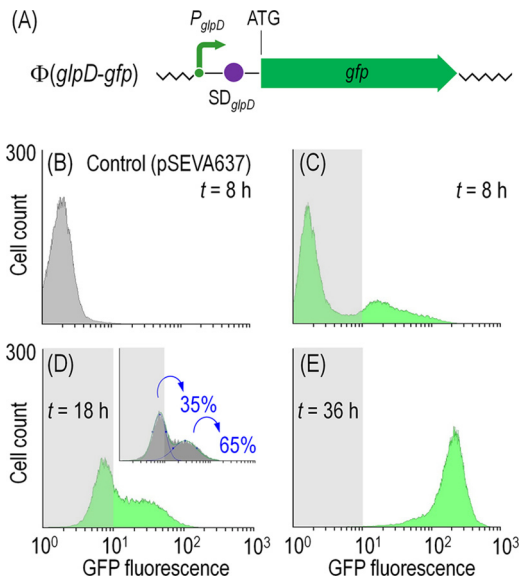
FIG 7 Transcriptional analysis of *glpD* expression in *P. putida* KT2440. (A) Schematic representation of the transcriptional Φ(*glpD-gfp*) fusion used to explore the expression of *glpD*. The 5′ untranslated region preceding *glpD* (which spans the P$_{glpD}$ promoter and a Shine-Dalgarno [SD] sequence [Fig. 1B]) was cloned into the pSEVA637 vector, which carries a promoter-less *gfp*, generating plasmid pTF-*glpD*. The elements in this outline are not drawn to scale. (B to E) Time-lapse of GFP fluorescence in *P. putida* KT2440 cells carrying the Φ(*glpD-gfp*) transcriptional fusion (plasmid pTF-*glpD*) and grown in shaken-flask cultures in M9 minimal medium containing glycerol as the sole carbon source. The gray rectangle in each plot identifies the region considered negative for the fluorescence signal (as assessed with cells carrying the empty pSEVA637 vector). The inset in panel D identifies the percentages of GFP⁻ and GFP⁺ cells as identified by analytical deconvolution of the raw flow cytometry data.

mately responsible for the bistable growth phenotype of *P. putida* KT2440 on glycerol. The next question was whether the transcription of the *glp* genes in a Δ*glpR* background also reflects the macroscopic effects observed in the mutant strain. We repeated the transcriptional assessment of the Φ(*glpD-gfp*) expression in *P. putida* Δ*glpR* and in the same strain complemented in *trans* with *glpR* (Fig. 8), using cells transformed with the empty pSEVA637 vector as the negative control (Fig. 8A). The transcription of *glpD* at 18 h in the mutant strain showed an entirely unimodal distribution (Fig. 8B), indicating that the transcription of Φ(*glpD-gfp*) becomes constitutive in the absence of the repressor protein in a fashion similar to what was observed in terms of the overall metabolic activity (Fig. 4) and the *in vitro* GlpK activity (Fig. 6B). This behavior was reverted by supplying *glpR* in an expression plasmid (Fig. 8C), and the resulting bimodal distribution mirrored the one observed for the wild-type strain under the same growth conditions (Fig. 7D). These results accredit the role of GlpR-dependent repression of the *glp* genes as the main cause of the phenotypic and growth properties of *P. putida* KT2440, drawing a direct correlation between the transcription of the *glp* genes, the enzymatic activity of the cognate catabolic pathway, and the overall physiology (as exposed by the duration of the lag phase) when cells are grown *en masse* on glycerol.

Increasing the intracellular glycerol-3-P content relieves the bimodal growth pattern on glycerol. The driving force for the uptake of glycerol is the substrate phosphorylation to G3P by GlpK (Fig. 1A and 6A). G3P, in turn, relieves the GlpR-associated repression of the *glp* genes in a positive feedback loop. We reasoned that this repression could also be lifted by artificially increasing the G3P pool. Is it possible for *P. putida* cells to transport G3P directly from the extracellular environment? A genomic anal-
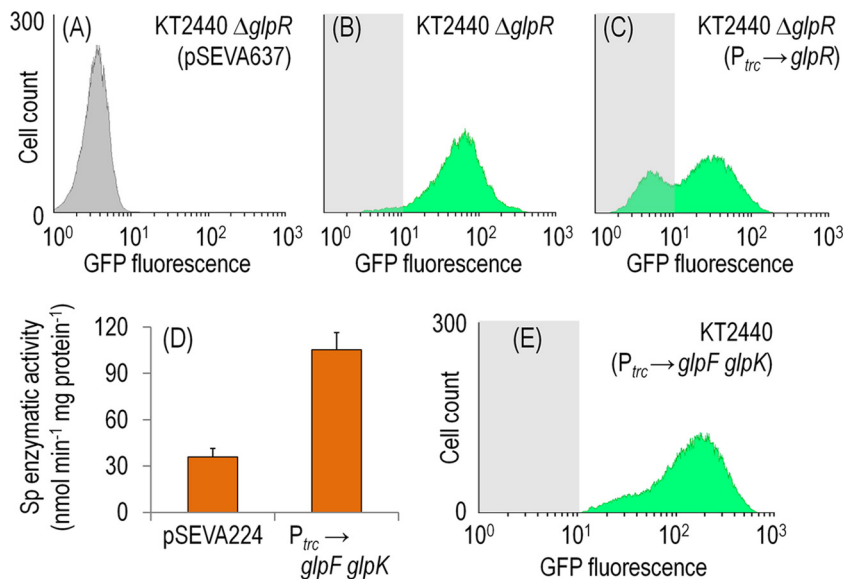

FIG 8 Role of GlpR repressor and of availability of glycerol-3-P in the expression of the *glp* genes in *P. putida*. (A to C) Transcriptional analysis of the expression of Φ(*glpD-gfp*) (carried on plasmid pTF-*glpD*) in the Δ*glpR* background at 18 h. Cells were grown in shaken-flask cultures using glycerol as the sole carbon source. The gray rectangle in each plot identifies the region considered negative for the fluorescence signal (as assessed with cells carrying the empty vector pSEVA637). (D) *In vitro* quantitation of the specific (Sp) GlpK enzymatic activity in the wild-type strain grown on glycerol and carrying the empty expression vector (pSEVA224) or overexpressing both *glpF* and *glpK* from plasmid pE-*glpFK*. Each bar represents the mean value of the corresponding enzymatic activity ± the standard deviation of duplicate measurements from at least three independent experiments. (E) GFP fluorescence in *P. putida* cells carrying the Φ(*glpD-gfp*) transcriptional fusion in the wild-type strain overexpressing both *glpF* and *glpK* after 18 h of growth in shaken-flask cultures using glycerol as the sole carbon source.

ysis of the *P. putida* KT2440 catalogue of glycerol-processing genes suggests that there are not specific transporters for this small molecule (26, 48), and when cells were incubated on M9 minimal medium containing G3P as the sole carbon source, no growth was observed (data not shown). An alternative possibility would be to boost the GlpK activity alone, but in this case, glycerol (the substrate for the kinase) might become limiting if the GlpF transporter (also dependent on GlpR) is not sufficiently active (49).

We attempted to increase the G3P input by overexpressing both *glpF* and *glpK* from strain KT2440 by cloning these genes in an expression plasmid (pSEVA224), giving rise to pE-*glpFK* (Table 1). Upon induction of the P$_{trc}$ promoter, which drives the expression of *glpF* and *glpK* with isopropyl-β-D-1-thiogalactopyranoside (IPTG), we measured the specific GlpK activity *in vitro* in glycerol cultures of the recombinants (Fig. 8D). The overexpression of *glpF* and *glpK* from plasmid pE-*glpFK* resulted in a 3-fold increase in the *in vitro* GlpK activity compared to a control experiment with *P. putida* KT2440 cells carrying the empty pSEVA224 vector. The activity values obtained for the control strain in this experiment are similar to those reported in Fig. 6B, indicating that the presence of the plasmid does not alter the *in vitro* GlpK activity. Although we did not measure the actual G3P concentration in these cells, it can be safely assumed that the turnover of this metabolite should be also increased in the strain overexpressing *glpK*, as observed in *Ralstonia eutropha* (49). We then explored the transcription level of the *glpD* gene using the transcriptional fusion described above (Fig. 7A) in glycerol cultures of the wild-type KT2440 strain overexpressing *glpF* and *glpK*. At 18 h, all the cells gave a positive signal for GFP in a unimodal fashion (Fig. 8E), similarly to the distribution observed in the Δ*glpR* mutant under the same growth conditions (Fig. 8B). This result indicates that the GlpR-dependent repression of the *glp* genes is relieved by increasing the intracellular G3P availability—demonstrating that G3P is the key metabolite that mediates the bistable phenotype of *P. putida* KT2440 on glycerol. When the analysis of single-cell batch cultures in microtiter plates was performed with these recombinant cells, the two subpopulations previously seen for the wild-type strain were not observed (data not shown). These results are in line with the notion that if cells are pregrown on glycerol (ensuring a sufficiently high G3P supply), the stochastic growth phenomenon is no longer observed.

Conclusion. Phenotypic variation within an otherwise genetically clonal population endows bacterial populations with functionalities that, under given particular circumstances, protect the genetic pool of the group under adverse conditions. The essence of the phenomenon is that either a genetic or a metabolic device generates differential expression of a certain trait, whether structural (e.g., phase variation of pathogens [50]), biochemical, or physiological. Pseudomonads exhibit such phenomena in the natural niches which they inhabit (17, 51). While virtually all prokaryotic promoters are subject to a degree of noise (52), certain regulatory architectures translate such noise into bi-/multimodal or bistable manifestation of the phenotype at stake in single cells. The ON/OFF ratio in these cases can be permanently set by a dedicated molecular device, or it can vary with time or other conditions. Each of these scenarios seems to have been selected to cope with evolutionary challenges and environmental stresses. A dramatic case is that of persister cells (22), which avoid killing by remaining in a static physiological state when most of the population succumbs to the action of antibiotics that target growing
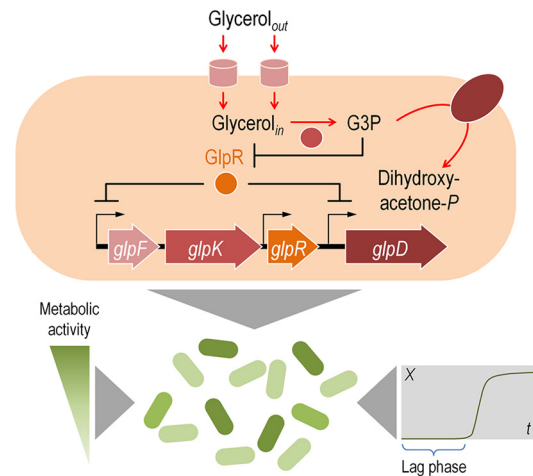

FIG 9 Proposed mechanism for the GlpR-mediated repression of the *glp* genes. The protracted lag phase observed in cultures of *P. putida* KT2440 growing in glycerol can be traced to the peculiar regulatory architecture of the *glp* genes, which needs the product of the first biochemical reaction (*sn*-glycerol-3-P [G3P]) for derepressing gene expression, which is otherwise inhibited by GlpR. Yet, since the genes encoding the glycerol transporter and the kinase that produces G3P are repressed themselves by the GlpR protein, the only way to get started is the low-probability effector-independent stochastic lifting of the repression. Once this repression is randomly overcome, the full expression of the *glp* genes can stably proceed—to finally return to an OFF state when glycerol is consumed. While the derepression process is taking place, this particular transcriptional architecture translates into different levels of metabolic activity (representing, in this context, the ability of the cells to catabolize glycerol). This situation, in turn, is macroscopically detected as a very long lag phase in a typical plot of biomass density (*X*) against time (*t*).

bacteria. In other instances, the same population splits into two or more groups that operate different portions of the same metabolic pathway (17).

In the scenario documented in this paper, the stochastic expression of genes needed for glycerol metabolism leads to a prolonged nongrowing state of most of the population of *P. putida* KT2440 when cells face this substrate (Fig. 9). Cells will start growing only if the low-probability effector-independent stochastic lifting of the GlpR-mediated repression allows for the expression of *glpF* and *glpK* (the latter being responsible for G3P formation). Once this repression is overcome stochastically, the full expression of the *glp* genes can proceed—finally returning to an OFF state when the substrate is completely depleted. Different levels of metabolic activity are observed in the cells (i.e., their ability to catabolize glycerol) while the transcriptional derepression process is occurring. This situation, in turn, explains the very long lag phase in mass *P. putida* cultures on glycerol. Along this line of reasoning, it has been recently shown that the level of activity of a given metabolic pathway (and the accumulation of critical metabolic intermediates stemming from it) governs the transition from a nongrowing to an actively growing state in bacteria and yeast (10–12).

What could be the advantage for bacteria holding such regulatory devices for glycerol metabolism? Glycerol is not an abundant carbon source in the environment, but it does appear, e.g., in root exudates in which pseudomonads are known to thrive (53, 54). As hexoses and organic acids seem to be the preferred carbon sources for *P. putida* (55–57), it could well happen that the prolonged inactivity of the cells when facing glycerol enables carbon source-

dependent metabolic bet hedging (58) to explore new chemical and nutritional landscapes. This concept is reminiscent of foraging in animal ecology (59, 60). In this case, some members of the population (but not the whole population) take risks to broaden the search for alternative food sources (61). Under this scheme, the cost of randomly expressing metabolic genes in *P. putida* is outweighed by the potential benefit of locating (and being prepared to utilize) alternative carbon sources. A similar situation was previously proposed for *E. coli* (62), based on the whole-population transcriptomic fingerprint of cells grown on different carbon sources. The concept is further refined by the results discussed in our contribution, in which the phenotypic cell-to-cell variations are taken into account and integrated into the foraging theory. While metabolic stochasticity may be beneficial in the environment (63), it certainly becomes a hurdle for the use of *P. putida* in a bioreactor setup as a microbial cell factory (64–66). In this sense, the present results suggest genetic strategies to bring about a coordinated consumption of glycerol as the carbon source in an industrial setting, where the polyol is becoming one of the preferred and most readily available substrates for biotechnology (67–69).

MATERIALS AND METHODS

Bacterial strains and growth conditions. The bacterial strains and the plasmids used in this study are listed in Table 1. *P. putida* and *E. coli* were routinely cultured in 250-ml Erlenmeyer flasks containing 50 ml of the corresponding culture medium with agitation at 170 rpm at either 30°C (*P. putida* strains) or 37°C (*E. coli* strains). For the propagation and construction of vectors, *E. coli* CC118 λ*pir* was cultured in LB medium (70) containing the appropriate antibiotics. Physiological experiments were carried out in M9 minimal medium (70, 71), containing 6 g · liter^{-1} Na$_2$HPO$_4$, 3 g · liter^{-1} KH$_2$PO$_4$, 1.4 g · liter^{-1} (NH$_4$)$_2$SO$_4$, 0.5 g · liter^{-1} NaCl, 0.2 g · liter^{-1} MgSO$_4$·7H$_2$O, and 2.5 ml · liter^{-1} of a trace element solution (72). Either 40 mM glycerol, 20 mM glucose, or 30 mM sodium succinate was added to M9 minimal medium as filter-sterilized solutions as the sole carbon source (i.e., the final medium contained 120 mM carbon atoms in all the experiments). Solid medium also contained 15 g · liter^{-1} agar. Antibiotics were added to medium when needed at the following final concentrations: ampicillin, 150 μg · ml^{-1} for *E. coli* strains or 500 μg · ml^{-1} for *P. putida* strains (used during mutant construction); kanamycin, 50 μg · ml^{-1}; and gentamicin, 15 μg · ml^{-1}. IPTG was used at 1.5 mM to induce the activity of the P$_{trc}$ promoter in overexpression experiments.

Growth experiment mixtures were inoculated with cells previously grown for 18 h in LB medium, previously spun, and washed twice with M9 minimal medium without any carbon source in order to remove any traces of nutrients from the rich culture medium. Note that since the final OD$_{600}$ achieved by *P. putida* cultures was different depending on whether the cells were cultured in Erlenmeyer flasks or microtiter plates, cultures were considered to have reached the mid-exponential phase of growth when their OD$_{600}$ values were roughly half the maximal cell density attained under that particular culture condition. Therefore, mid-exponential cells were harvested at an OD$_{600}$ of 0.3 in microtiter plate cultures and at an OD$_{600}$ of 0.5 in shaken-flask cultures. Microtiter plate cultures were inoculated with one *P. putida* cell as follows. Precultures, washed and finally resuspended in M9 minimal medium without any carbon substrate as described above, were adjusted to an OD$_{600}$ in such a way that by addition of 5 μl of the bacterial suspension to 195 μl of fresh M9 minimal medium (previously added with the corresponding carbon source), each well would contain 1 *P. putida* cell in a final volume of 200 μl. Under these growth conditions, the maximal OD$_{600}$ values attained by all cultures were not very different and always less than 1 unit. Calibration curves were routinely run to correlate the OD$_{600}$ of a culture and the cell density (measured as the number of *P. putida* cells per micro-

liter) (73, 74). Kinetic parameters, such as the duration of the lag phase, were calculated as described previously (26), and in all cases, the mean value of the corresponding parameter is given along with the standard deviation calculated from at least five technical replicates in four independent experiments.

General genetic techniques and mutant construction. Unless otherwise stated, DNA manipulations followed well-established methods (70) and specific recommendations from manufacturers. Oligonucleotides were purchased from Sigma-Aldrich Co. (St. Louis, MO), and their sequences are listed in Table S1 in the supplemental material. A *P. putida* KT2440 Δ*glpR* mutant was constructed using the method of allelic replacement described by Martínez-García and de Lorenzo (75), with oligonucleotides Δ*glpR*-TS1-F, Δ*glpR*-TS1-R, Δ*glpR*-TS2-F, and Δ*glpR*-TS2-R.

Cloning of the *glpD* promoter into the *gfp* reporter plasmid pSEVA637. The *glpD* promoter was identified by *in silico* searching of conserved motifs in the 5′ untranslated region within the *glp* gene cluster (35). The promoter was amplified by PCR from chromosomal DNA of *P. putida* KT2440 using oligonucleotides *glpD*-TF-EcoRI-F and *glpD*-TF-BamHI-R listed in Table S1 in the supplemental material. The 236-bp amplicon was digested and cloned as an EcoRI-BamHI fragment upstream of *gfp* into the multiple cloning site of pSEVA637. After transformation into *E. coli* CC118 λ*pir*, plasmids were isolated and the correct transcriptional Φ(*glpD-gfp*) fusion was verified by PCR, restriction analysis, and sequencing (Secugen SL, Madrid, Spain). The resulting Φ(*glpD-gfp*) reporter vector, termed pTF-*glpD*, was introduced into *P. putida* KT2440 and its Δ*glpR* mutant by triparental mating (76), using *E. coli* HB101/pRK600 (Table 1) as the helper strain.

Overexpression of *glpF* and *glpK* as a synthetic operon and construction of a *glpR* complementation plasmid. A synthetic operon, comprising *glpF* and *glpK*, was constructed by crossover (sewing) PCR (77). A first fragment, comprising *glpF*, was amplified using genomic DNA from *P. putida* KT2440 as the template and oligonucleotides *glpF*-EcoRI-F and *glpF*-R. The *glpK* gene was separately amplified with oligonucleotides *glpK*-F and *glpK*-SacI-R. Finally, sewing PCR amplification was used to generate the synthetic operon using a mixture of the amplification products from the first and second PCR steps as the template and the external oligonucleotides (i.e., *glpF*-EcoRI-F and *glpK*-SacI-R). The 2,392-bp amplicon spanned the *glpF* and *glpK* genes as a single transcriptional unit bracketed by EcoRI and SacI restriction sites, with a Shine-Dalgarno motif included before the ATG codon of each gene. This fragment was cloned into the expression vector pSEVA224 (LacI^q/P$_{trc}$) digested with the same enzymes, giving rise to plasmid pE-*glpFK*. A similar procedure was used to construct an expression plasmid for *glpR* complementation. In this case, genomic DNA from *P. putida* KT2440 was used as the template in a PCR amplification using oligonucleotides *glpR*-EcoRI-F and *glpR*-BamHI-R. The 797-bp amplicon was digested with EcoRI and BamHI and cloned into pSEVA224, resulting in plasmid pE-*glpR*.

Fluorescence microscopy, image analysis, and flow cytometry. *Bac*Light RedoxSensor Green (RSG) vitality staining was used to diagnose the metabolic state of individual cells. The signal intensity of cells stained with the RSG reagent is altered when cells are treated with reagents that disrupt electron transport (such as NaN$_3$), and we resorted to this compound to run negative controls in each set of experimental samples. *P. putida* reacted significantly to the addition of 10 mM NaN$_3$. In each set of experiments, 10^6 cells suspended in 0.5 ml of phosphate-buffered saline (PBS) buffer (70) were stained with 1 μl of the RSG solution provided by Life Technologies Corp. (Grand Island, NY). Staining procedures followed the instructions of the manufacturer. In some experiments, cells were also stained with propidium iodide to evaluate vitality. Bacteria with damaged cell membranes represented a very small population (<10%) during logarithmic growth in all the carbon sources tested, and excluding this subpopulation by gating on the propidium iodide-negative population did not alter the distribution of RSG subpopulations (data not shown). For immobilization of the cells in microscopy experiments, 2 μl

of the cell suspension was placed onto 0.01% (wt/vol) poly-L-lysine (Sigma-Aldrich Co.)-coated coverslips and dried. Then, each coverslip was assembled with a slide including Prolong (Life Technologies Corp.) to suppress photobleaching and sealed using clear nail polish. Microscopy was performed using an Olympus BX61 microscope equipped with a 100× phase-contrast objective and a DP70 camera (Olympus Corp., Tokyo, Japan). GFP signals were measured using wide-field excitation with an MNIBA2 fluorescence mirror unit. We resorted to our in-house software coded in Python (Python Software Foundation, Delaware) for image analysis read and explored all the pixels within the fluorescence microscopy images, reading and quantifying the information from the green channel. We used the Python Imaging Library (PIL) and Matplotlib to plot the results.

Flow cytometry methods followed well-established protocols specifically adapted to *P. putida* (66, 72, 76, 78), analyzing at least 25,000 cells under each experimental condition. Analysis of flow cytometry data was conducted using Cyflogic 1.2.1 software (CyFlo Ltd., Turku, Finland). Histogram plots have a measure of fluorescence intensity shown on the *x* axis and the number of bacteria (i.e., events) counted at the specific fluorescence intensity used for RSG/GFP detection shown on the *y* axis.

***In vitro* quantitation of the GlpK activity.** The GlpK assay mixture contained (in a final volume of 1.0 ml) 2.5 mM ATP, 3 mM glycerol, 0.5 mM NAD$^+$, 0.8 M hydrazine monohydrate buffer (pH 10.4), 125 mM glycine buffer (pH 8.5), 2 mM MgCl$_2$, 4.5 U α-glycerol-3-P dehydrogenase from rabbit muscle (Sigma-Aldrich Co.), and 80 to 200 μl of the cell extract obtained from cells harvested during exponential growth (OD$_{600}$ of ca. 0.5). Preparation of cell extracts and other analytical procedures were described in previous publications (26, 72, 76, 79).

SUPPLEMENTAL MATERIAL

Supplemental material for this article may be found at http://mbio.asm.org/lookup/suppl/doi:10.1128/mBio.00340-15/-/DCSupplemental.

Figure S1, PDF file, 0.1 MB.
Figure S2, PDF file, 0.1 MB.
Figure S3, PDF file, 0.1 MB.
Table S1, PDF file, 0.03 MB.
Table S2, PDF file, 0.03 MB.

REFERENCES

1. de Lorenzo V. 2014. From the selfish gene to selfish metabolism: revisiting the central dogma. Bioessays **36**:226–235. http://dx.doi.org/10.1002/bies.201300153.
2. de Lorenzo V, Sekowska A, Danchin A. 16 September 2014. Chemical reactivity drives spatiotemporal organisation of bacterial metabolism. FEMS Microbiol Rev http://dx.doi.org/10.1111/1574-6976.12089.
3. Brehm-Stecher BF, Johnson EA. 2004. Single-cell microbiology: tools, technologies, and applications. Microbiol Mol Biol Rev **68**:538–559. http://dx.doi.org/10.1128/MMBR.68.3.538-559.2004.
4. Czechowska K, Johnson DR, van der Meer JR. 2008. Use of flow cytometric methods for single-cell analysis in environmental microbiology. Curr Opin Microbiol **11**:205–212. http://dx.doi.org/10.1016/j.mib.2008.04.006.
5. Heinemann M, Zenobi R. 2011. Single cell metabolomics. Curr Opin Biotechnol **22**:26–31. http://dx.doi.org/10.1016/j.copbio.2010.09.008.
6. Kortmann H, Blank LM, Schmid A. 2011. Single cell analytics: an over-view. Adv Biochem Eng Biotechnol **124**:99–122. http://dx.doi.org/10.1007/10_2010_96.
7. de Jong IG, Veening JW, Kuipers OP. 2012. Single cell analysis of gene expression patterns during carbon starvation in *Bacillus subtilis* reveals large phenotypic variation. Environ Microbiol **14**:3110–3121. http://dx.doi.org/10.1111/j.1462-2920.2012.02892.x.
8. Afroz T, Biliouris K, Kaznessis Y, Beisel CL. 2014. Bacterial sugar utilization gives rise to distinct single-cell behaviours. Mol Microbiol **93**:1093–1103. http://dx.doi.org/10.1111/mmi.12695.
9. Kröger C, Srikumar S, Ellwart J, Fuchs TM. 2011. Bistability in *myo*-inositol utilization by *Salmonella enterica* serovar Typhimurium. J Bacteriol **193**:1427–1435. http://dx.doi.org/10.1128/JB.00043-10.
10. Kotte O, Volkmer B, Radzikowski JL, Heinemann M. 2014. Phenotypic bistability in *Escherichia coli*'s central carbon metabolism. Mol Syst Biol **10**:736. http://dx.doi.org/10.15252/msb.20135022.
11. van Heerden JH, Wortel MT, Bruggeman FJ, Heijnen JJ, Bollen YJ, Planqué R, Hulshof J, O'Toole TG, Wahl SA, Teusink B. 2014. Lost in transition: start-up of glycolysis yields subpopulations of nongrowing cells. Science **343**:1245114. http://dx.doi.org/10.1126/science.1245114.
12. Solopova A, van Gestel J, Weissing FJ, Bachmann H, Teusink B, Kok J, Kuipers OP. 2014. Bet-hedging during bacterial diauxic shift. Proc Natl Acad Sci U S A **111**:7427–7432. http://dx.doi.org/10.1073/pnas.1320063111.
13. Lidstrom ME, Konopka MC. 2010. The role of physiological heterogeneity in microbial population behavior. Nat Chem Biol **6**:705–712. http://dx.doi.org/10.1038/nchembio.436.
14. Kaern M, Elston TC, Blake WJ, Collins JJ. 2005. Stochasticity in gene expression: from theories to phenotypes. Nat Rev Genet **6**:451–464. http://dx.doi.org/10.1038/nrg1615.
15. Smits WK, Kuipers OP, Veening JW. 2006. Phenotypic variation in bacteria: the role of feedback regulation. Nat Rev Microbiol **4**:259–271. http://dx.doi.org/10.1038/nrmicro1381.
16. Veening JW, Smits WK, Kuipers OP. 2008. Bistability, epigenetics, and bet-hedging in bacteria. Annu Rev Microbiol **62**:193–210. http://dx.doi.org/10.1146/annurev.micro.62.081307.163002.
17. Nikel PI, Silva-Rocha R, Benedetti I, de Lorenzo V. 2014. The private life of environmental bacteria: pollutant biodegradation at the single cell level. Environ Microbiol **16**:628–642. http://dx.doi.org/10.1111/1462-2920.12360.
18. Dubnau D, Losick R. 2006. Bistability in bacteria. Mol Microbiol **61**:564–572. http://dx.doi.org/10.1111/j.1365-2958.2006.05249.x.
19. Koirala S, Mears P, Sim M, Golding I, Chemla YR, Aldridge PD, Rao CV. 2014. A nutrient-tunable bistable switch controls motility in *Salmonella enterica* serovar typhimurium. mBio **5**(5):e01611-14. http://dx.doi.org/10.1128/mBio.01611-14.
20. Lewis K. 2010. Persister cells. Annu Rev Microbiol **64**:357–372. http://dx.doi.org/10.1146/annurev.micro.112408.134306.
21. Balaban NQ, Gerdes K, Lewis K, McKinney JD. 2013. A problem of persistence: still more questions than answers? Nat Rev Microbiol **11**:587–591. http://dx.doi.org/10.1038/nrmicro3076.
22. Balaban NQ, Merrin J, Chait R, Kowalik L, Leibler S. 2004. Bacterial persistence as a phenotypic switch. Science **305**:1622–1625. http://dx.doi.org/10.1126/science.1099390.
23. Arnoldini M, Vizcarra IA, Peña-Miller R, Stocker N, Diard M, Vogel V, Beardmore RE, Hardt WD, Ackermann M. 2014. Bistable expression of virulence genes in *Salmonella* leads to the formation of an antibiotic-tolerant subpopulation. PLoS Biol **12**:e1001928. http://dx.doi.org/10.1371/journal.pbio.1001928.
24. Clarke PH. 1982. The metabolic versatility of pseudomonads. Antonie van Leeuwenhoek **48**:105–130. http://dx.doi.org/10.1007/BF00405197.
25. Lessie TG, Phibbs PV, Jr. 1984. Alternative pathways of carbohydrate utilization in pseudomonads. Annu Rev Microbiol **38**:359–388. http://dx.doi.org/10.1146/annurev.mi.38.100184.002043.
26. Nikel PI, Kim J, de Lorenzo V. 2014. Metabolic and regulatory rearrangements underlying glycerol metabolism in *Pseudomonas putida* KT2440. Environ Microbiol **16**:239–254. http://dx.doi.org/10.1111/1462-2920.12224.
27. Kim J, Oliveros JC, Nikel PI, de Lorenzo V, Silva-Rocha R. 2013. Transcriptomic fingerprinting of *Pseudomonas putida* under alternative physiological regimes. Environ Microbiol Rep **5**:883–891. http://dx.doi.org/10.1111/1758-2229.12090.
28. Lin EC. 1976. Glycerol dissimilation and its regulation in bacteria. Annu

Rev Microbiol **30**:535–578. http://dx.doi.org/10.1146/annurev.mi.30.100176.002535.

29. **Booth IR**. 2005. Glycerol and methylglyoxal metabolism. EcoSal Plus http://dx.doi.org/10.1128/ecosalplus.3.4.3.

30. **Tsay SS, Brown KK, Gaudy ET**. 1971. Transport of glycerol by *Pseudomonas aeruginosa*. J Bacteriol **108**:82–88.

31. **Escapa IF, Del Cerro C, García JL, Prieto MA**. 2013. The role of GlpR repressor in *Pseudomonas putida* KT2440 growth and PHA production from glycerol. Environ Microbiol **15**:93–110. http://dx.doi.org/10.1111/j.1462-2920.2012.02790.x.

32. **Rawls KS, Yacovone SK, Maupin-Furlow JA**. 2010. GlpR represses fructose and glucose metabolic enzymes at the level of transcription in the haloarchaeon *Haloferax volcanii*. J Bacteriol **192**:6251–6260. http://dx.doi.org/10.1128/JB.00827-10.

33. **Schweizer HP**. 1991. The *agmR* gene, an environmentally responsive gene, complements defective *glpR*, which encodes the putative activator for glycerol metabolism in *Pseudomonas aeruginosa*. J Bacteriol **173**:6798–6806.

34. **Schweizer HP, Po C**. 1996. Regulation of glycerol metabolism in *Pseudomonas aeruginosa*: characterization of the *glpR* repressor gene. J Bacteriol **178**:5215–5221.

35. **Danilova LV, Gel'fand MS, Liubetskiĭ VA, Laĭkova ON**. 2003. Computer analysis of regulating metabolism of glycerol-3-phosphate in proteobacteria genome. Mol Biol (Mosk) **37**:843–849. http://dx.doi.org/10.1023/A:1026037027266.

36. **Neidhardt FC, Ingraham JL, Schaechter M**. 1990. Physiology of the bacterial cell: a molecular approach. Sinauer Associates, Sunderland, MA.

37. **Madar D, Dekel E, Bren A, Zimmer A, Porat Z, Alon U**. 2013. Promoter activity dynamics in the lag phase of *Escherichia coli*. BMC Syst Biol **7**:136. http://dx.doi.org/10.1186/1752-0509-7-136.

38. **Hogg RV, Tanis EA, Zimmerman D**. 2014. Probability and statistical inference, 8th ed. Pearson Prentice Hall, Upper Saddle River, NJ.

39. **Kalyuzhnaya MG, Lidstrom ME, Chistoserdova L**. 2008. Real-time detection of actively metabolizing microbes by redox sensing as applied to methylotroph populations in Lake Washington. ISME J **2**:696–706. http://dx.doi.org/10.1038/ismej.2008.32.

40. **Konopka MC, Strovas TJ, Ojala DS, Chistoserdova L, Lidstrom ME, Kalyuzhnaya MG**. 2011. Respiration response imaging for real-time detection of microbial function at the single-cell level. Appl Environ Microbiol **77**:67–72. http://dx.doi.org/10.1128/AEM.01166-10.

41. **Nielsen TH, Sjøholm OR, Sørensen J**. 2009. Multiple physiological states of a *Pseudomonas fluorescens* DR54 biocontrol inoculant monitored by a new flow cytometry protocol. FEMS Microbiol Ecol **67**:479–490. http://dx.doi.org/10.1111/j.1574-6941.2008.00631.x.

42. **Müller S, Nebe-von-Caron G**. 2010. Functional single-cell analyses: flow cytometry and cell sorting of microbial populations and communities. FEMS Microbiol Rev **34**:554–587. http://dx.doi.org/10.1111/j.1574-6976.2010.00214.x.

43. **Romero-Campero FJ, Pérez-Jiménez MJ**. 2008. Modelling gene expression control using *P* systems: the *lac* operon, a case study. Biosystems **91**:438–457. http://dx.doi.org/10.1016/j.biosystems.2007.02.011.

44. **Berthoumieux S, de Jong H, Baptist G, Pinel C, Ranquet C, Ropers D, Geiselmann J**. 2013. Shared control of gene expression in bacteria by transcription factors and global physiology of the cell. Mol Syst Biol **9**:634. http://dx.doi.org/10.1038/msb.2012.70.

45. **Bouvet OM, Lenormand P, Ageron E, Grimont PA**. 1995. Taxonomic diversity of anaerobic glycerol dissimilation in the *Enterobacteriaceae*. Res Microbiol **146**:279–290. http://dx.doi.org/10.1016/0923-2508(96)81051-5.

46. **Schweizer HP, Jump R, Po C**. 1997. Structure and gene-polypeptide relationships of the region encoding glycerol diffusion facilitator (*glpF*) and glycerol kinase (*glpK*) of *Pseudomonas aeruginosa*. Microbiology **143**:1287–1297. http://dx.doi.org/10.1099/00221287-143-4-1287.

47. **Choi PJ, Cai L, Frieda K, Xie XS**. 2008. A stochastic single-molecule event triggers phenotype switching of a bacterial cell. Science **322**:442–446. http://dx.doi.org/10.1126/science.1161427.

48. **Nelson KE, Weinel C, Paulsen IT, Dodson RJ, Hilbert H, Martins dos Santos VA, Fouts DE, Gill SR, Pop M, Holmes M, Brinkac L, Beanan M, DeBoy RT, Daugherty S, Kolonay J, Madupu R, Nelson W, White O, Peterson J, Khouri H, Hance I, Chris Lee P, Holtzapple E, Scanlan D, Tran K, Moazzez A, Utterback T, Rizzo M, Lee K, Kosack D, Moestl D, Wedler H, Lauber J, Stjepandic D, Hoheisel J, Straetz M, Heim S, Kiewitz C, Eisen JA, Timmis KN, Düsterhöft A, Tümmler B, Fraser CM**. 2002. Complete genome sequence and comparative analysis of the meta-

49. bolically versatile *Pseudomonas putida* KT2440. Environ Microbiol **4**:799–808. http://dx.doi.org/10.1046/j.1462-2920.2002.00366.x.

49. **Fukui T, Mukoyama M, Orita I, Nakamura S**. 2014. Enhancement of glycerol utilization ability of *Ralstonia eutropha* H16 for production of polyhydroxyalkanoates. Appl Microbiol Biotechnol **98**:7559–7568. http://dx.doi.org/10.1007/s00253-014-5831-3.

50. **Casadesús J, Low DA**. 2013. Programmed heterogeneity: epigenetic mechanisms in bacteria. J Biol Chem **288**:13929–13935. http://dx.doi.org/10.1074/jbc.R113.472274.

51. **van den Broek D, Bloemberg GV, Lugtenberg B**. 2005. The role of phenotypic variation in rhizosphere *Pseudomonas* bacteria. Environ Microbiol **7**:1686–1697. http://dx.doi.org/10.1111/j.1462-2920.2005.00912.x.

52. **Elowitz MB, Levine AJ, Siggia ED, Swain PS**. 2002. Stochastic gene expression in a single cell. Science **297**:1183–1186. http://dx.doi.org/10.1126/science.1070919.

53. **Badri DV, Vivanco JM**. 2009. Regulation and function of root exudates. Plant Cell Environ **32**:666–681. http://dx.doi.org/10.1111/j.1365-3040.2008.01926.x.

54. **Carvalhais LC, Dennis PG, Fedoseyenko D, Hajirezaei M, Borriss R, von Wirén N**. 2011. Root exudation of sugars, amino acids, and organic acids by maize as affected by nitrogen, phosphorus, potassium, and iron deficiency. J Plant Nutr Soil Sci **174**:3–11. http://dx.doi.org/10.1002/jpln.201000085.

55. **Chavarría M, Kleijn RJ, Sauer U, Pflüger-Grau K, de Lorenzo V**. 2012. Regulatory tasks of the phosphoenolpyruvate-phosphotransferase system of *Pseudomonas putida* in central carbon metabolism. mBio **3**(2):e00028-12. http://dx.doi.org/10.1128/mBio.00028-12.

56. **Chavarría M, Nikel PI, Pérez-Pantoja D, de Lorenzo V**. 2013. The Entner-Doudoroff pathway empowers *Pseudomonas putida* KT2440 with a high tolerance to oxidative stress. Environ Microbiol **15**:1772–1785. http://dx.doi.org/10.1111/1462-2920.12069.

57. **Nikel PI, Martínez-García E, de Lorenzo V**. 2014. Biotechnological domestication of pseudomonads using synthetic biology. Nat Rev Microbiol **12**:368–379. http://dx.doi.org/10.1038/nrmicro3253.

58. **de Jong IG, Haccou P, Kuipers OP**. 2011. Bet hedging or not? A guide to proper classification of microbial survival strategies. Bioessays **33**:215–223. http://dx.doi.org/10.1002/bies.201000127.

59. **Beckerman A, Petchey OL, Morin PJ**. 2010. Adaptive foragers and community ecology: linking individuals to communities and ecosystems. Funct Ecol **24**:1–6. http://dx.doi.org/10.1111/j.1365-2435.2009.01673.x.

60. **Mangel M, Clark CW**. 1986. Towards a unified foraging theory. Ecology **67**:1127–1138. http://dx.doi.org/10.2307/1938669.

61. **Brown JS, Laundré JW, Gurung M**. 1999. The ecology of fear: optimal foraging, game theory, and trophic interactions. J Mammal **80**:385–399. http://dx.doi.org/10.2307/1383287.

62. **Liu M, Durfee T, Cabrera JE, Zhao K, Jin DJ, Blattner FR**. 2005. Global transcriptional programs reveal a carbon source foraging strategy by *Escherichia coli*. J Biol Chem **280**:15921–15927. http://dx.doi.org/10.1074/jbc.M414050200.

63. **Ackermann M**. 2013. Microbial individuality in the natural environment. ISME J **7**:465–467. http://dx.doi.org/10.1038/ismej.2012.131.

64. **Delvigne F, Goffin P**. 2014. Microbial heterogeneity affects bioprocess robustness: dynamic single-cell analysis contributes to understanding of microbial populations. Biotechnol J **9**:61–72. http://dx.doi.org/10.1002/biot.201300119.

65. **Ruiz JA, de Almeida A, Godoy MS, Mezzina MP, Bidart GN, Méndez BS, Pettinari MJ, Nikel PI**. 2012. *Escherichia coli* redox mutants as microbial cell factories for the synthesis of reduced biochemicals. Comput Struct Biotechnol J **3**:e201210019. http://dx.doi.org/10.5936/csbj.201210019.

66. **Martínez-García E, Nikel PI, Aparicio T, de Lorenzo V**. 2014. *Pseudomonas* 2.0: genetic upgrading of *P. putida* KT2440 as an enhanced host for heterologous gene expression. Microb Cell Fact **13**:159. http://dx.doi.org/10.1186/s12934-014-0159-3.

67. **da Silva GP, Mack M, Contiero J**. 2009. Glycerol: a promising and abundant carbon source for industrial microbiology. Biotechnol Adv **27**:30–39. http://dx.doi.org/10.1016/j.biotechadv.2008.07.006.

68. **Murarka A, Dharmadi Y, Yazdani SS, González R**. 2008. Fermentative utilization of glycerol by *Escherichia coli* and its implications for the production of fuels and chemicals. Appl Environ Microbiol **74**:1124–1135. http://dx.doi.org/10.1128/AEM.02192-07.

69. **Yazdani SS, González R**. 2007. Anaerobic fermentation of glycerol: a path

to economic viability for the biofuels industry. Curr Opin Biotechnol **18:** 213–219. http://dx.doi.org/10.1016/j.copbio.2007.05.002.

70. **Green MR, Sambrook J**. 2012. Molecular cloning: a laboratory manual, 4th ed. Cold Spring Harbor Laboratory, Cold Spring Harbor, NY.

71. **Nikel PI, de Almeida A, Pettinari MJ, Méndez BS**. 2008. The legacy of HfrH: mutations in the two-component system CreBC are responsible for the unusual phenotype of an *Escherichia coli arcA* mutant. J Bacteriol **190:** 3404–3407. http://dx.doi.org/10.1128/JB.00040-08.

72. **Nikel PI, de Lorenzo V**. 2013. Engineering an anaerobic metabolic regime in *Pseudomonas putida* KT2440 for the anoxic biodegradation of 1,3-dichloroprop-1-ene. Metab Eng **15:**98–112. http://dx.doi.org/10.1016/j.ymben.2012.09.006.

73. **Gilbert P, Brown MR, Costerton JW**. 1987. Inocula for antimicrobial sensitivity testing: a critical review. J Antimicrob Chemother **20:**147–154. http://dx.doi.org/10.1093/jac/20.2.147.

74. **Koch AL**. 2007. Growth measurement, p 172–199. In Reddy CA, Beveridge TJ, Breznak JA, Marzluf GA, Schmidt TM, Snyder LR (ed), Methods for general and molecular microbiology, 3rd ed. ASM Press, Washington, DC.

75. **Martínez-García E, de Lorenzo V**. 2011. Engineering multiple genomic deletions in Gram-negative bacteria: analysis of the multi-resistant antibiotic profile of *Pseudomonas putida* KT2440. Environ Microbiol **13:** 2702–2716. http://dx.doi.org/10.1111/j.1462-2920.2011.02538.x.

76. **Nikel PI, de Lorenzo V**. 2013. Implantation of unmarked regulatory and metabolic modules in Gram-negative bacteria with specialised mini-transposon delivery vectors. J Biotechnol **163:**143–154. http://dx.doi.org/10.1016/j.jbiotec.2012.05.002.

77. **Horton RM, Cai ZL, Ho SN, Pease LR**. 1990. Gene splicing by overlap extension: tailor-made genes using the polymerase chain reaction. Biotechniques **8:**528–535.

78. **Martínez-García E, Nikel PI, Chavarría M, de Lorenzo V**. 2014. The metabolic cost of flagellar motion in *Pseudomonas putida* KT2440. Environ Microbiol **16:**291–303. http://dx.doi.org/10.1111/1462-2920.12309.

79. **Martínez-García E, Aparicio T, de Lorenzo V, Nikel PI**. 2014. New transposon tools tailored for metabolic engineering of Gram-negative microbial cell factories. Front Bioeng Biotechnol **2:**46. http://dx.doi.org/10.3389/fbioe.2014.00046.

80. **Herrero M, de Lorenzo V, Timmis KN**. 1990. Transposon vectors containing non-antibiotic resistance selection markers for cloning and stable chromosomal insertion of foreign genes in Gram-negative bacteria. J Bacteriol **172:**6557–6567.

81. **Boyer HW, Roulland-Dussoix D**. 1969. A complementation analysis of the restriction and modification of DNA in *Escherichia coli*. J Mol Biol **41:**459–472. http://dx.doi.org/10.1016/0022-2836(69)90288-5.

82. **Bagdasarian M, Lurz R, Rückert B, Franklin FC, Bagdasarian MM, Frey J, Timmis KN**. 1981. Specific-purpose plasmid cloning vectors. II. Broad host range, high copy number, RSF1010-derived vectors, and a host-vector system for gene cloning in *Pseudomonas*. Gene **16:**237–247. http://dx.doi.org/10.1016/0378-1119(81)90080-9.

83. **Kessler B, Herrero M, Timmis KN, de Lorenzo V**. 1994. Genetic evidence that the XylS regulator of the *Pseudomonas* TOL *meta* operon controls the *Pm* promoter through weak DNA-protein interactions. J Bacteriol **176:**3171–3176.

84. **Silva-Rocha R, Martínez-García E, Calles B, Chavarría M, Arce-Rodríguez A, de las Heras A, Páez-Espino AD, Durante-Rodríguez G, Kim J, Nikel PI, Platero R, de Lorenzo V**. 2013. The Standard European Vector architecture (SEVA): a coherent platform for the analysis and deployment of complex prokaryotic phenotypes. Nucleic Acids Res **41:** D666–D675. http://dx.doi.org/10.1093/nar/gks1119.

85. **Martínez-García E, Aparicio T, Goñi-Moreno A, Fraile S, de Lorenzo V**. 2015. SEVA 2.0: an update of the Standard European Vector architecture for de-/re-construction of bacterial functionalities. Nucleic Acids Res **43:** D1183–D1189. http://dx.doi.org/10.1093/nar/gku1114.